S. Bhattacharya · R. Kar

High-temperature dehydration melting and decompressive P–T path in a granulite complex from the Eastern Ghats, India

Abstract The granulite complex of Paderu, in the south central sector of the Eastern Ghats belt, India, consists of closely related pelitic granulites and peraluminous granitoids which could be linked via dehydration melting in pelitic and greywacke-like precursors. The pelitic granulites, including high-Mg-Al sapphirine granulites with early deformation microstructures, also record a high-temperature decompression from ~10 to ~8 kbar at ~1,000 °C, preceding isobaric cooling from above 900 to ~600 °C at 8 kbar. Highly magnesian biotite in the pelitic granulites, the presence of spinel in some of the granitoids, and granitoids of two distinct compositions, namely granite and quartz-monzonite, all suggest dehydration melting in highly magnesian pelitic and greywacke-like precursors. Moreover, high-temperature melting in highly magnesian pelitic precursors is indicated by the migmatitic spinel-bearing layers which, besides having significant abundance of quartz and feldspar, also contain aluminous orthopyroxene and cordierite. These melting reactions, occurring above 9 kbar, may constrain the prograde arm of the P–T trajectory. This and the high-temperature decompression constitute a clockwise P–T path. This clockwise P–T path is consistent with the tectonic model in which crustal thickening and granulite metamorphism in the Eastern Ghats belt is interpreted as the result of homogeneous shortening in a compressional setting.

Introduction

High-grade metapelites following a clockwise P–T path as a result of crustal thickening-related heating commonly undergo dehydration melting due to decomposition of micas (Stevens and Clemens 1993; Brown 1994). Also, Raith et al. (1997) described high-temperature assemblage coexisting with melt from a south Indian locality. Some recent experiments have indicated high-temperature (≥900 °C) dehydration melting in high-Mg pelitic and greywacke precursors (Carrington and Harley 1995a; Stevens et al. 1997). The high-Mg-Al sapphirine granulites with symplectitic reaction textures have been described from different granulite terrains and are commonly interpreted as indicative of a decompressive P–T path (Harley and Fitzsimons 1991; Nichols and Berry 1991; Mohan and Windley 1993; Harley 1998).

In the Eastern Ghats granulite belt along the east coast of India, dehydration melting in pelitic precursors under granulite facies conditions has been reported from several localities, although in these cases melting occurred at around 800–850 °C (Dasgupta et al. 1992; Sen and Bhattacharya 1997, 2000). A decompressive P–T path has also been described from some areas in the Eastern Ghats belt (Lal et al. 1987; Sen et al. 1995; Mohan et al. 1997). However, opinion is sharply divided on the question of a clockwise or counter-clockwise P–T path for the metamorphic evolution of the granulites of the Eastern Ghats belt (Sengupta et al. 1990; Sen et al. 1995; Bhattacharya 1996; Mukhopadhyay and Bhattacharya 1997; Mohan et al. 1997). These proposed P–T paths have profound implications on the tectonic evolution of granulite complexes in regional granulite terrains like the Eastern Ghats belt.

In this study we report high-temperature dehydration melting in high-Mg pelitic and greywacke precursors, linking the orthopyroxene-free granitoids with the intimately associated metapelitic granulites from an area in the south-central sector of the Eastern Ghats belt, India.

Additionally, we record a high-temperature decompressive P–T path from the high-Mg metapelitic assemblages from the study area, which is compatible with a clockwise P–T trajectory. Finally, we discuss the implications of the clockwise P–T path for the tectonic evolution of the granulite complex of the area in relation to that of the Eastern Ghats granulite belt.

Geological setting

The study area, around Paderu in Andhra Pradesh (Fig. 1, inset) in the south central sector of the Eastern Ghats granulite belt, exposes metapelitic granulites including khondalites and high-Mg-Al sapphirine granulites, mafic granulites, charnockite-enderbites and orthopyroxene-free granitoids.

The effects of three phases of folding are observed in the granulite-granitoid complex (Fig. 1). F_1 folds, locally present as intrafolial folds, are represented by quartzite bands in khondalites and mafic granulite bands within massif-type charnockite-enderbite bodies. F_2 folds occur on various scales and largely determine the map pattern. F_2 folds are commonly overturned with N-S axial traces and variable but steep plunges. F_3 folds are mostly broad warps with E-W axial traces. S_1 gneissosity, axial planar to intrafolial F_1 folds, is represented by segregation banding in khondalites and streaky gneissic foliation in the charnockite-enderbites. S_2 gneissosity, defined by elongate quartz-feldspar aggregates, is axial planar to F_2 folds in khondalites and charnockite-enderbites. S_3 foliation is only locally developed as fracture cleavage in khondalites and as crenulation cleavage axial planar to F_3 folds in charnockite-enderbites and granite-gneisses.

Besides the dominant metapelitic granulites (khondalites) in the eastern and western sectors of the study area, high-Mg-Al sapphirine granulites generally occur as small blocks (less than 50×50 cm) within massif-type charnockite-enderbite bodies and granites and also as folded bands (or layers) within massif-type charnockite-enderbite (Fig. 1). It is important to note that these high-Mg-Al sapphirine granulites contain evidence of early deformation structures (S_1), and hence their disposition in low strain zones is similar to those described from Antarctica by Harley et al. (1990). The orthopyroxene-free granitoids, closely associated with metapelitic granulites, occur as stock-like bodies and also interlayered with the metapelitic granulites.

Petrography

Metapelitic granulites can be grouped into three distinct types based on mineral assemblage. Common metapelitic granulites, the so-called khondalites, have the assemblage Grt–Sil–Qtz–Kfs–Ilm (type P-I). The mineral abbreviations in this paper are after Kretz (1983). Graphite, although usually taken to be ubiquitous, is not observed in the khondalites of the present area. Instead, aluminous spinel is locally present. Also, unlike the khondalites of other areas in the Eastern Ghats belt (cf. Sen and Bhattacharya 1997, 2000), some samples contain plagioclase feldspars, indicating the presence of greywacke-like protoliths in the area. The absence of prograde biotite and the occasional presence of quartzofeldspathic pods in the khondalites suggest their restitic nature, from which partial melt had presumably been extracted.

High-Mg-Al metapelites (type P-II), occur as small blocks or enclaves within charnockitic gneisses and also as thin layers within granitic gneisses. The characteristic assemblage is Opx–Crd–Spr–Sil–Qtz–Bio. Garnet is locally observed in thin layers which lack orthopyroxene. The highly refractory nature of this assemblage is suggestive of their restitic nature.

The layered bodies with a distinct foliation, occurring within charnockitic and granitic gneisses (type P-III), have three distinct assemblages: (1) Opx–Crd–Spr–Sil–Osm–Bio–Qtz–Kfs; (2) Opx–Spl–Spr–Sil–Osm–Bio–Qtz–Kfs; and (3) Opx–Spl–Spr–Crd–Sil–Bio–Osm–Qtz–Kfs. These layered bodies can also be described as quartzofeldspathic gneisses, but the presence of minerals like sillimanite, cordierite, spinel and osumilite indicate their affinity to pelitic precursors.

The granitoids, occurring as small plutons/stocks or bands, have a distinctive foliation defined by elongate quartz-feldspar ribbons, the so-called leptynitic foliation. Mineralogically, three varieties can be recognised: granite with garnet as the common ferromagnesian phase (G-I); granite with spinel, instead of garnet, as the common ferromagnesian phase (G-II); and quartz-monzonite with garnet and/or biotite as the common ferromagnesian phase (G-III). Sillimanite trails and biotite inclusions within some garnets suggest pelitic precursors of these granitoids. Precursor of quartz-monzonite, on the other hand, could be greywacke-like.

Mineral compositions

Minerals were analysed on a Jeol Jxa-8600 M microprobe at the USIC, University of Roorkee, India. 15-kV accelerating voltage, 2×10^{-8} amp sample current and 2-μm beam diameter were used.

Sapphirine

Sapphirine is aluminous, Al_2O_3 varying between 59.6 and 64.4 wt% (Table 1). The sapphirine is stoichiometric and shows solid solution according to the substitution (Mg, Fe^{2+}) + Si⇔2(Al, Fe^{3+}, Cr), with very little Cr, and plots near a line joining 7:9:3 and 2:2:1 in [(Mg, Fe)O: Al_2O_3:SiO_2] molar proportions. The present sapphirine is closer to 7:9:3 (Fig. 2). Sapphirine crystals are of variable compositions, particularly in their magnesium contents. Two generations of sapphirine could be identified with distinct compositions. Symplectitic sapphirine (in P-II

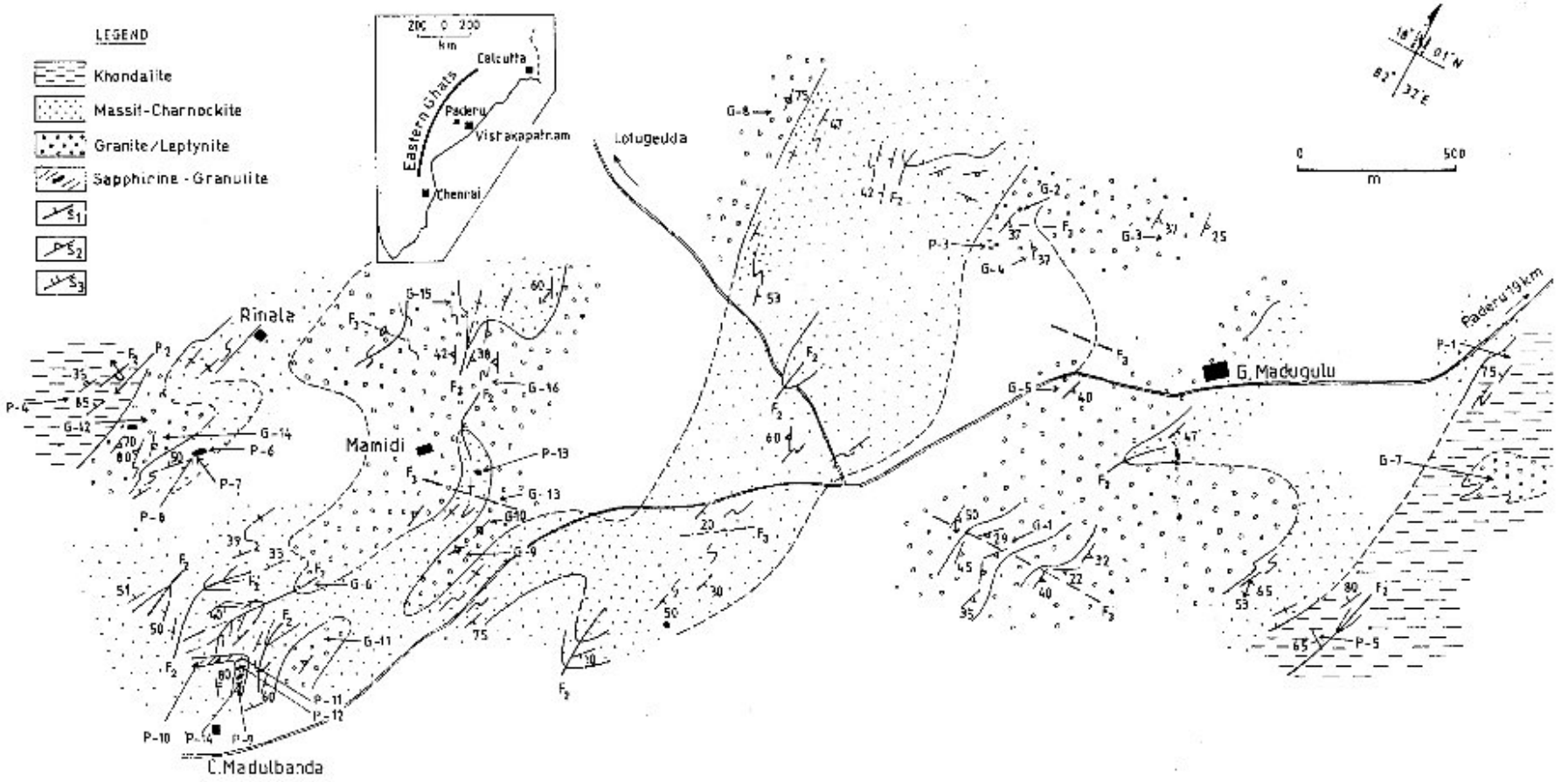

Fig. 1. Simplified geological map of the granulite complex of Paderu, Andhra Pradesh, showing sample locations. *P* Pelites, *G* granitoids

Table 1. Representative sapphirine composition

Rock type	P-IIIa		P-II		P-IIIc		P-IIIb	P-II	
Sample no.	46b		10c		15c		49	31b	
Ref. no.	C1/12c	C1/13r	C1/1	C2/2	C1/4c	C1/5r	C2/16	C2/2c	C2/1r
SiO_2	13.63	13.65	14.4	14.31	10.48	10.94	12.25	12.94	13.64
Al_2O_3	60.82	60.89	60.79	60.6	64.42	63.71	64.04	62.18	62.24
FeO	6.6	6.86	5.02	5.03	7.86	7.86	7.49	6.07	6.24
MgO	18.17	17.75	16.95	18.14	15.36	15.27	16.87	17.05	16.87
MnO	0.05	0.1	0.009	0.08	0.11	0.06	–	0.11	0.1
K_2O	0.001	–	–	–	–	0.03	0.01	–	0.02
TiO_2	0.03	0.01	–	–	0.03	0.04	0.05	0.03	0.01
Cr_2O_3	0.04	–	–	–	0.05	0.03	–	0.04	0.04
Total	99.341	99.26	97.169	98.16	98.31	97.94	100.71	98.42	99.16
X_{Mg}	0.83	0.82	0.86	0.87	0.78	0.78	0.8	0.83	0.83

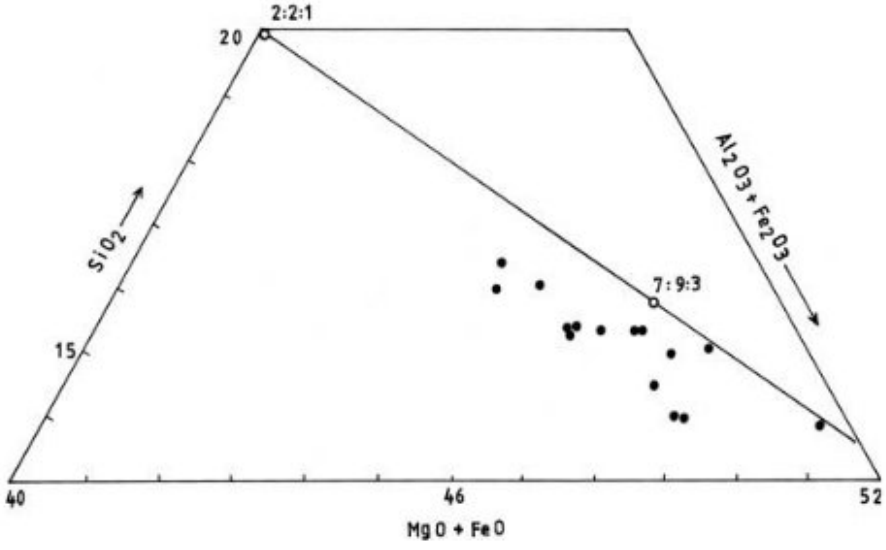

Fig. 2. Sapphirine compositions recalculated to include Fe_2O_3, and plotted in part of the SiO_2–(Mg,Fe)O–$(Al,Fe)_2O_3$ diagram (molar proportions)

and P-IIIa) with cordierite (X_{Mg}^{Spr} 0.82–0.83) and orthopyroxene (X_{Mg}^{Spr} 0.83–0.87) is more magnesian than that produced from spinel in spinel-bearing assemblages, either coronal growth (X_{Mg}^{Spr} 0.72–0.78) or porphyroblastic (X_{Mg}^{Spr} 0.80) in P-IIIb and P-IIIc.

Spinel

Spinel is primarily spinel-hercynite solid solution with very little magnetite and gahnite components (Table 2). Fe is mainly reduced, with $Fe^{+2}/(Fe^{+2}+Fe^{+3})$ of 0.95 to 0.96. This and the small abundance of other components like Cr and Zn is compatible with that of a FMAS phase (Nichols et al. 1992). X_{Mg} varies between 0.48 and 0.53 and is less magnesian than coexisting Opx (X_{Mg} 0.72–0.75), Spr (X_{Mg} 0.72–0.80), Bio (X_{Mg} 0.86) and Crd (X_{Mg} 0.89). Spinel in granitoids (G-II) is also aluminous, similar to those in the metapelitic assemblages P-IIIb and c but of more ferroan compositions (X_{Mg} 0.27–0.33).

Cordierite

Cordierite is mostly dry, as indicated by relatively high totals (above 98 wt%) and absence of alkalies (Vry et al. 1990). Calculated formulae, based on 18 oxygen, show Si consistently above 5 (mean of +0.11) and Al consistently below 4 (mean of –0.16). This is consistent with the mechanism of substitution proposed by Schreyer et al. (1990), namely $Si^{+} \Leftrightarrow Al^{+}$ (Na, K), except that alkalies are lacking in the cordierite here (Table 3). Again, the variation of cation totals in formulae based on 18 oxygen, 11 ± 0.06, can be related to deviation of (Fe, Mg) stoichiometry, 2 ± 0.06. Two analyses in P-IIIa, sample 97/46b (C2/3, C2/4), representing core and rim compositions, are clearly contaminated by quartz inclusion, as in the experiment of Vielzeuf and Montel (1994). Otherwise, cordierite is unzoned and is the most magnesian phase (X_{Mg} 0.89–0.94). Also, there is subtle difference of X_{Mg} in the two assemblages, namely 0.89 in the spinel-bearing assemblage (P-IIIc) and 0.91–0.94 in the spinel-absent assemblage (P-II).

Table 2. Representative spinel and ilmenite compositions (spinel, ilmenite/Mgt)

Rock type	P-IIIc		P-IIIb		G-II			G-I
Sample no.	95/15c		97/49		97/67(mt)			95/2 (ilm)
Ref. no.	C1/1	C3/8	C2/18	C2/19	C1/1	C1/2	C1/3	C1/5
SiO_2	–	–	–	–	–	–	–	–
Al_2O_3	56.81	57.71	57.7	55.77	53.83	51.26	0.34	0.07
TiO_2	–	–	–	–	0.02	–	0.21	38.66
FeO	24.75	24.76	24.03	26.95	32.83	36.59	93.58	43.05
MgO	14.77	14.53	14.68	13.32	7.77	7.4	0.05	2.42
MnO	0.05	–	0.15	0.01	0.19	0.18	–	0.1
Cr_2O_3	–	0.03	0.08	0.03	0.06	–	–	–
ZnO	0.22	0.1	0.24	0.25	0.17	0.004	–	–
CaO	–	–	–	–	0.74	0.28	0.59	0.61
Total	96.6	97.13	96.88	96.33	95.61	95.714	94.77	84.91
X_{Mg}	0.53	0.52	0.53	0.48	0.33	0.27	–	–

Table 3. Representative cordierite composition in metapelites

Rock type	P-IIIa				P-II		P-II				P-IIIb		
Sample no.	97/46b				97/31b		95/10c				97/49		
Ref. no.	C1/1	C2/3	C2/4	C3/5	C1/1	C1/2	C1/1	C4/4	C5/3	C1/7	C1/8	C3/9	C3/10
SiO_2	51.75	62.07	63.21	51.75	50.24	51.15	51.14	51.24	52.03	50.59	57.4	50.8	51.77
Al_2O_3	33.41	25.94	26.17	33.45	33.01	33.03	33.05	33.33	33.97	32.71	27.86	32.66	32.95
TiO_2	–	0	0.03	0	0.03	0.01	0	0	0	0.06	0.02	0.04	0.07
FeO	2.51	1.88	1.74	2.66	2.22	1.94	1.7	1.57	1.67	2.75	1.72	3.32	3.35
MgO	13.16	10.42	10.41	13.5	12.86	12.17	12.6	12.42	12.66	12.57	8.15	12.36	12.71
MnO	0.05	0.04	0.02	0.02	0.04	0.09	0.05	0	0.1	0	0.01	0.08	0.01
Total	100.9	100.4	101.6	101.4	98.55	98.39	98.54	98.55	100.4	98.68	95.16	99.3	100.8
X_{Mg}	0.91	0.91	0.91	0.9	0.91	0.92	0.93	0.93	0.93	0.89	0.89	0.87	0.87

Orthopyroxene

Orthopyroxene in both the high-Mg-Al metapelitic assemblages is aluminous, the spinel-bearing assemblages (P-IIIb, c) with 5.83 to 18.34% Al_2O_3 and the spinel-absent association (P-II and P-IIIa) with 6.3 to 9.3% Al_2O_3 (Table 4). The high Al_2O_3 in orthopyroxene reflects more aluminous bulk compositions and hence the starting rocks are metapelitic, rather than metagreywackes (Stevens et al. 1997). Of the two assemblages, the spinel-bearing assemblage has orthopyroxene of much variable and higher Al_2O_3 contents. It is important to note that rimward zoning in Al_2O_3, with more aluminous cores (8.43 to 16.38 wt% at the cores and 6.13 to 13.41 wt% at the rim), is marked. Such rimward decrease in Al_2O_3 in orthopyroxene is reported from Antarctica (Harley et al. 1990) and South Africa (Dawson et al. 1997), and also from the Eastern Ghats belt (Lal et al. 1987; Sengupta et al. 1990). The decrease of Al_2O_3 towards the rim suggests pressure drop (Harley 1984; Montel and Vielzeuf 1997) and is compatible with orthopyroxene produced in successive reactions with the same X_{Mg} in the spinel-absent assemblages (P-II, P-IIIa). In terms of magnesium content, orthopyroxene in the two assemblages is of distinct composition – the spinel-absent assemblages (P-II and P-IIIa) have orthopyroxene of more magnesian composition (X_{Mg} 0.78 to 0.84) than that of the spinel-bearing assemblages (X_{Mg} 0.72 to 0.80).

Biotite

Unlike the primary biotite of similar high-Mg sapphirine granulites from Forefinger Point, Antarctica (Harley et al. 1990), the present biotite is less aluminous (Al_2O_3~13 wt%) and compares well with those described by Lal et al. (1987). However, the variation in TiO_2 reported by Lal et al. (1987; between 1.6 and 4.9 wt%) as being a possible effect of re-equilibration during retrograde reactions is not observed in biotite of the present study (Table 5). Present biotites have nearly constant TiO_2 (~4 wt%). Structural formulae based on 22 oxygen show variation of octahedral Al between 0.19 and 0.65. The correlation of Al^6 and (Fe + Mg) agrees well with the substitution proposed by Patino Douce et al. (1993), namely $0.66Al^6 + 0.33^R = Fe, Mg$. Present biotite is highly magnesian (X_{Mg} 0.86 to 0.90). Biotites in the spinel-absent assemblages (P-II, IIIa) are more magnesian (X_{Mg} 0.89–0.90) than those of the spinel-bearing assemblage P-IIIb, c (X_{Mg} 0.86). Also, biotite in orthopyroxene-free domains (97/17c) is similar to that in orthopyroxene-containing domains (95/15c), with

Table 4. Representative orthopyroxene composition

Rock type	P-IIIa			P-II		P-IIIc		P-IIIb				P-II	
Sample no.	46b			10c		15c		49		31b		17b	
Ref. no.	C4/29	C2/25	C4/30	C1/1	C1/2	C1/8	C1/9	C1/31	C3/33	C1/1c	C1/2r	C1/1	C3/4
SiO_2	50.4	50.7	50	53.5	52.3	51.6	51.8	52.13	48.57	50.77	50.26	51.57	50.23
TiO_2	0.08	0.05	0.12	–	–	0.08	0.07	0.07	0.14	0.13	0.12	0.09	0.11
Al_2O_3	7.9	8.96	9.3	6.98	6.86	14	6.13	6.03	8.46	8.65	8.72	7.54	8.37
FeO	13.9	11.2	13	10.1	10.5	13.7	16.3	15.84	16.59	13.38	13.37	16	16.55
MnO	0.4	0.22	0.24	0.29	0.23	0.12	0.01	0.06	0.15	0.27	0.35	0.27	0.31
MgO	28	28.1	28.8	30.3	30	19.4	27	26.34	26.31	26.86	26.18	25.97	23.26
CaO	0.05	0.04	0.02	0.05	0.01	0.05	0.02	0.05	0.04	0.04	0.08	0.06	0.07
Na_2O		0.01	0	0	0	0.1	0	0	0	0	0	0.19	0
K_2O	0.02	–	0.01	–	0.07	0.02	0.01	–	0.02	–	0	–	–
Cr_2O_3	–	–	0	–	0	–	0	–	0	–	0	–	–
Total	101	99.3	102	101	100	99	101	100.52	100.27	100.1	99.07	101.69	98.9
X_{Mg}	0.78	0.81	0.8	0.84	0.84	0.72	0.74	0.75	0.74	0.78	0.78	0.74	0.71

Table 5. Representative biotite composition

Sample no.	95/15c		97/31b			97/17b		97/17c		97/67		97/3			
Rock type	P-III		P-II			P-II		P-II		G-II		G-I			
Ref. no.	C4/5	C4/6	C1/9	C2/11	C5/13	C1/1	C2/3	C1/1	C2/3	C2/7	C3/8	C1/10	C2/2	C2/5	C3/1
SiO_2	40.9	41.42	40.41	41.03	41.66	40.81	41.49	39.65	42.17	40.93	41.64	36.17	37.47	37.35	38.48
Al_2O_3	13.15	13.88	13.33	13.34	13.03	12.77	12.99	12.75	14.22	11.52	12.24	13.1	13.8	13.77	13.47
TiO_2	4.92	4.13	4.19	4.32	3.85	4.35	3.78	4.42	4.71	3.92	1.97	3.38	3.38	4.35	3.93
FeO	6.71	6.72	4.62	4.58	4.49	6.52	5.94	5.69	5.43	9.09	4.54	10.09	10.24	10.48	9.95
MnO	–	0.05	0.04	0.02	0.02	0.04	0.02	0.01	0.004	0.04	–	0.04	0.03	0.04	0.06
MgO	23.99	23.54	21.99	21.72	22.67	23.23	24.82	20.3	21.11	20.06	22.92	18.02	16.95	18.09	18.19
CaO	0.01	0.03	–	–	–	–	–	–	0	–	–	0.01	0.01	0.01	0.05
Na_2O	0.06	0.11	0.52	0.35	0.18	0.3	0.23	0.28	0.15	0.07	0.14	0.04	0.17	0.1	0.22
K_2O	9.69	9.63	9.93	10.06	10.3	9.4	9.74	8.94	9.55	10.02	10.11	10.16	9.43	10.11	10.31
Total	99.43	99.51	95.03	95.42	96.2	97.42	99.01	92.04	97.344	95.65	93.56	91	91.47	94.29	94.71
X_{Mg}	0.86	0.86	0.89	0.89	0.9	0.86	0.88	0.86	0.87	0.8	0.9	0.76	0.75	0.76	0.77
Al^6	0.26	0.34	0.46	0.51	0.43	0.28	0.19	0.54	0.65	0.31	0.3	0.37	0.58	0.46	0.46
Fe, Mg	5.68	5.58	5.23	5.13	5.28	5.61	5.78	5.15	4.99	5.42	5.48	5.45	5.15	5.31	5.22
Al^6/Ti	0.51	0.791	1.02	1.11	1.05	2.17	0.49	1.1	1.33	0.721	1.43	0.95	1.49	0.94	1.05

$X_{Mg} = 0.86–0.87$ in both. In the spinel-bearing granites (G-II), the biotite is highly magnesian (Table 5), X_{Mg} varying between 0.80 and 0.90 (sample no. 97/67), whereas those in garnet-bearing granite (G-I) are less magnesian but still mainly phlogopite (X_{Mg} 0.75–77). Highly magnesian biotites in the granitoids, although they could be restitic, possibly indicate magnesian bulk composition of their protoliths.

Osumilite

Relict osumilite within symplectitic intergrowths could be identified under the microscope, and it is found to be uniaxial positive with low birefringence (~0.01), and colourless with one set of distinct cleavage (cf. below). However, our efforts to obtain microprobe analyses failed to produce good results, presumably due to the beam hitting submicroscopic intergrowths. We report here reconstituted osumilite analyses, using the composition of the intergrowth phases by mass balance calculations (Table 6). It is important to note that reconstituted osumilite is of different composition in the two assemblages P-IIIb and c, with higher X_{Mg} (0.81) in P-IIIb in which it coexists with cordierite, and lower X_{Mg} (0.74) in P-IIIc which lacks cordierite.

Garnet

Garnet is found in small domains in the high-Mg-Al spinel-absent pelitic assemblage (P-II) which is free of orthopyroxene (thin layers). However, coexisting biotite in this domain is of identical composition (X_{Mg} 0.86) to that in the adjacent orthopyroxene-bearing layers, which incidentally also have minor sapphirine. Also, orthopyroxene in this adjacent domain, lacking garnet, is of identical composition (X_{Mg} 0.74) to that of the spinel-absent pelitic assemblage (P-II). Although garnet is not detected as a coexisting phase with orthopyroxene and cordierite, biotite and orthopyroxene compositions in adjacent domains are indirect evidence that garnet-orthopyroxene-cordierite could have coexisted at some stage in the evolution of these granulite assemblages. In this context, it is interesting to note that the garnet

Table 6. Compositions of minerals in intergrowth textures around relic osumilite

Rock type	P-IIIb			P-IIIc			
Oxides Sample/ref. no.	Opx 15c/C1-14	Kfs 15c/C1-1	Osu[a] 15c/C1-15	Opx 49/C4-33	Kfs 49/C4-4	Crd 49/C4-7	Osu[a] 49/C4-23
SiO_2	52.16	64.61	63.07	48.57	67.35	50.59	61.96
Al_2O_3	8.69	19.7	22.23	8.46	18.75	32.71	24.48
FeO	15.34	–	4.39	16.59	–	2.75	2.80
MgO	24.12	–	6.91	26.31	–	12.57	6.52
MnO	0.12	–	–	0.15	–	–	–
CaO	–	0.03	–	0.04	0.10	–	0.04
Na_2O	0.03	1.85	0.45	–	2.35	–	0.89
K_2O	0.04	12.22	2.93	0.02	8.67	–	3.30
Total	100.5	98.41	99.98	100.14	97.22	98.62	99.99
X_{Mg}	0.74	–	0.74	0.74	–	0.89	0.81

[a]Osumilite could not be analysed properly and is here calculated/reconstituted from intergrowth phases. Two osumilite breakdown reactions 5 and 6 are indicated by textures in the two samples 15c and 49 respectively

composition here (X_{Mg} 0.45–0.47) is identical to that from the Grt_{47}–Opx_{72}–Crd_{89} assemblage of the Chilka area (Sen et al. 1995). Garnet in G-I type of granitoid is almandine-pyrope (Alm_{57}–Prp_{43}) and is similar to that in the P-II metapelitic assemblage (Table 7).

Feldspar

Plagioclase is generally absent in all the pelitic assemblages here, although some were optically identified in some khondalites (P-I). The alkali feldspar is commonly high sanidine with X_{Na} varying between 0.15 and 0.30 (Table 8). All the granite varieties contain plagioclase of andesine (An_{31-40}) compositions. The alkali feldspars are commonly perthitic, $Or_{83}Ab_{16}$ to $Or_{79}Ab_{19}$; but high-sanidine/anorthoclase grains are also common in spinel-bearing granites (G-II) ($Or_{53}Ab_{40}An_7$ to $Or_{58}Ab_{37}An_5$), and occasionally in the G-I type of granite ($Or_{44}Ab_{46}An_{10}$). Common occurrences of high-sanidine/anorthoclase in the granites and in some metapelites are the likely results of high-temperature melting and/or crystallisation.

Table 7. Representative garnet composition in metapelite and granite

Rock type	P-II			G-I	
Sample no.	97/17c			95/2	
Ref. no.	C1/1	C2/3	C2/4	C1/7	C2/10
SiO_2	36.98	40.11	40.18	39.2	39.32
Al_2O_3	21.68	22.47	22.38	21.83	22.62
FeO	21.55	25.17	25.29	26.77	25.73
MgO	11.62	12.27	11.81	11.42	11.22
MnO	0.52	0.59	0.64	0.61	0.69
CaO	0.54	0.71	0.64	1.14	1.31
TiO_2	0.04	0.05	–	–	–
Total	92.93	101.37	100.94	100.97	100.89
X_{Mg}	0.48	0.45	0.44	0.41	0.41

Metamorphic reactions

The growth of cordierite on corroded orthopyroxene, with relict sillimanite (Fig. 3a) and cordierite separating orthopyroxene and sillimanite indicate a reaction such as

$$Opx + 2Sil + Qtz = Crd \quad (1)$$

The common occurrence of sapphirine-cordierite symplectites with relict orthopyroxene inclusions (Fig. 3b) and sapphirine-cordierite symplectites on corroded margin of orthopyroxene (Fig. 3c) indicate a reaction such as

$$3.3Opx + 7Sil = 2.6Crd + 0.2Spr(7:9:3) \quad (2)$$

Here, it is important to note that the present sapphirine is closer to 7:9:3 (Fig. 2), and that this reaction was originally described by Lal (1997).

The breakdown of early cordierite is indicated by coarse orthopyroxene-sapphirine symplectites at the margin of cordierite (Fig. 3d), and this suggests the reaction

$$9Crd = 2Opx + 2Spr(7:9:3) + 35Qtz \quad (3)$$

The reaction textures attesting to reactions are observed in the two assemblages P-II and P-IIIa with distinct phase compositions, possibly reflecting differences in bulk composition discussed below.

In the spinel-bearing assemblages (P-IIIb, c), reaction textures attesting to sapphirine produced from spinel are common. The common occurrence of coronal sapphirine on spinel and on spinel-quartz association (Fig. 4a) indicates a reaction such as

$$7Spl + 2Sil + Qtz = Spr(7:9:3) \quad (4a)$$

This reaction predicts sillimanite as a reactant phase, and this is confirmed in Fig. 4b in which sapphirine isolates spinel from quartz and sillimanite in the matrix.

Partial coronas of sapphirine and quartz on spinel with relict orthopyroxene in the adjacent matrix (Fig. 4c)

Table 8. Representative feldspar composition in metapelites and granites

Rock type	P-IIIa		P-IIIb				P-IIIc			P-II		G-II			G-III		G-I			
Sample no.	97/46a		97/49		97/47		95/15c			97/31b		97/35b			97/67		95/2		97/3	
Ref. no.	C2/4	C3/1	C2/5	C2/6	C2/4	C2/10	C1/1	C1/3	C1/4	C5/9	C5/10	C1/1	C1/3	C2/1	C3/3	C1/5	C1/6	C1/1c	C1/2r	C3/4
SiO_2	64.78	64.73	67.42	65.64	66.48	66.83	64.61	66.71	67.35	66.57	65.97	63.81	60.66	66.46	66.18	66.11	65.58	58.44	59.77	58.13
Al_2O_3	19.56	19.01	18.46	20.15	18.29	17.33	19.7	19.15	18.75	18.74	18.19	17.68	22.36	19.47	19.25	18.35	20.32	26.57	26.56	26.19
CaO	0.05	0.04	0.08	0.05	0.03	0.03	0.03	0.06	0.09	0.28	0.15	0.16	6.31	1.38	1.04	0.18	1.97	6.45	6.91	6.69
K_2O	1.87	2.25	13.19	11.17	1.68	1.99	12.22	12.01	8.67	11.7	12.83	13.87	0.22	9.37	10.06	13.33	7.5	7.58	6.48	7.61
Na_2O	13.49	13.14	2.12	2.03	14.34	13.77	1.85	2.24	2.35	3.29	2.16	1.74	5.14	4.66	4.27	2.15	5.24	0.7	0.55	0.75
Total	100.27	99.54	101.27	99.04	101.33	100.32	98.41	100.17	97.21	100.58	99.3	97.26	94.69	101.34	100.8	100.12	100.61	100.17	100.63	99.79
X_{Ca}	0.002	0	0	0	0	0	0	0	0	0.01	0.01	0.01	0.4	0.07	0.05	0.02	0.1	0.31	0.36	0.31
X_{Na}	0.18	0.21	0.19	0.22	0.15	0.18	0.19	0.22	0.3	0.3	0.2	0.16	0.59	0.4	0.37	0.19	0.46	0.65	0.61	0.65
X_K	0.82	0.79	0.81	0.78	0.85	0.82	0.81	0.78	0.7	0.69	0.79	0.83	0.01	0.53	0.58	0.79	0.44	0.04	0.03	0.04

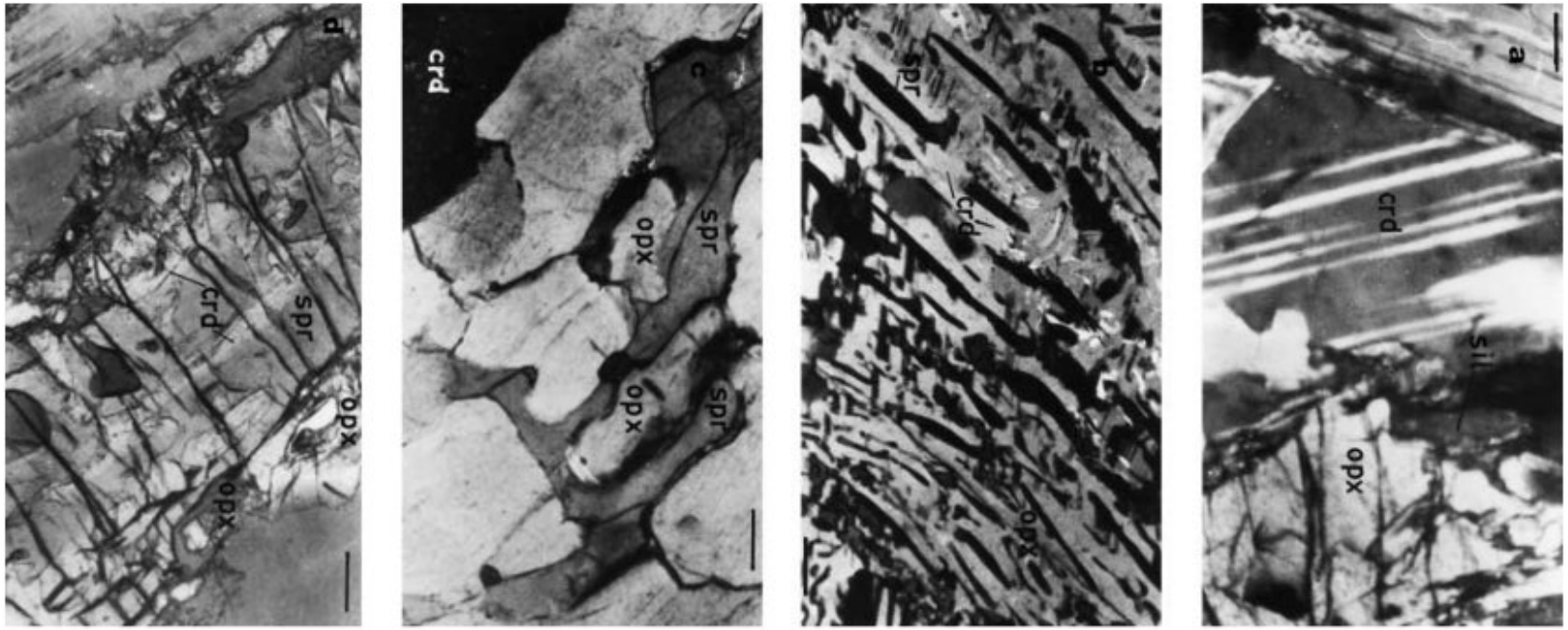

and sapphirine-quartz association separating orthopyroxene and spinel (Fig. 4d) suggest another sapphirine-forming reaction:

◄

Fig. 3a–d. Photomicrographs (*scale bars* = 7 μ). **a** Cordierite at corroded margins of orthopyroxene with relict sillimanite. **b** Cordierite-sapphirine symplectites with orthopyroxene inclusion. **c** Sapphirine-cordierite symplectites on corroded margins of orthopyroxene. **d** Coarse orthopyroxene-sapphirine symplectites at the margin of cordierite

$$5Spl + Opx + 4Sil = Spr(7:9:3) + 3Qtz \quad (4b)$$

In the P-IIIc assemblage, plumose intergrowths of cordierite-orthopyroxene-K-feldspar are common and occasionally enclose relict osumilite (Fig. 5a). This can be taken to indicate an osumilite breakdown reaction such as

$$3Osm = Opx + 2Crd + 3Kfls + 7Qtz \quad (5)$$

Another osumilite breakdown reaction in the assemblage P-IIIb is indicated by orthopyroxene-sillimanite-K-feldspar intergrowth enclosing relict osumilite (Fig. 5b), such as

$$Osm = Opx + 2Sil + Kfls + 3Qtz \quad (6)$$

Pressure-temperature constraints

In spite of the fact that highly magnesian pelitic assemblages preserve early mineral assemblages in several granulite belts, and the refractory nature of the minerals prevent their destruction during subsequent deformation and thermal perturbation, geothermobarometric estimates from these mineral assemblages are plagued by several difficulties. The most important constraint is related to thermochemical computation with inconsistent data sets, in particular for phases like sapphirine for which no calorimetric data exist. Sen et al. (1995), therefore, derived thermochemical parameters for sapphirine from the internally consistent database of Berman (1988). Using the same principle, thermochemical parameters for sapphirine (7:9:3) are retrieved from the internally consistent data base of Holland and Powell (1990), via several reactions involving cordierite, enstatite, spinel, sillimanite and quartz (Table 9).

New calibrations

Reaction 1.

$$P\ (bar) = 11.87 \times T - 4{,}546.30 - 1.85 \times T \times \ln k,$$

where $k = a_{Crd}/a_{Opx}$.

►

Fig. 4a–d. Photomicrographs (*scale bars* = 7 μ). **a** Coronal sapphirine on spinel and spinel-quartz association. **b** Sapphirine isolates spinel from quartz and sillimanite. **c** Partial corona of sapphirine and quartz on spinel with relict orthopyroxene in the adjacent matrix. **d** Sapphirine-quartz association separates orthopyroxene and spinel

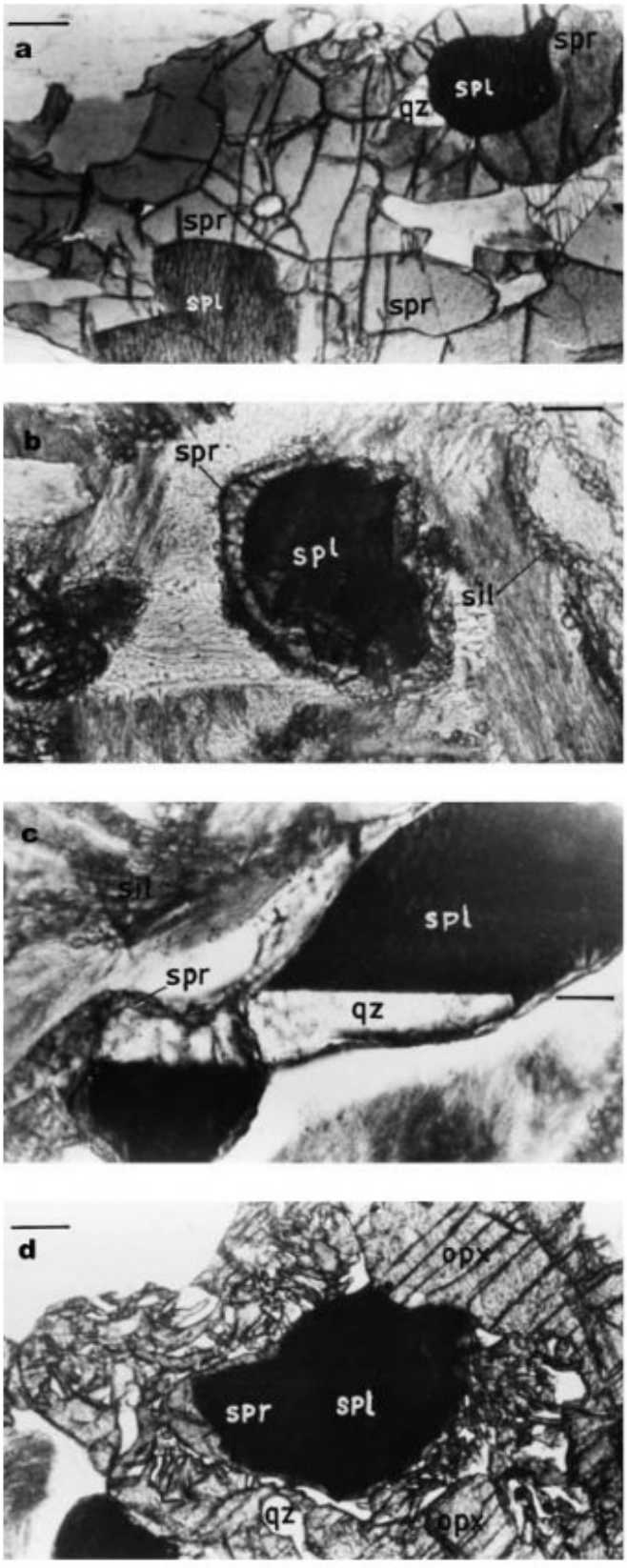

Reaction 2.

$$T\ (°K) = [27{,}660 + 14.74 \times P\ (bar)]/[132.49 - 8.313 \times \ln k],$$

where $k = [(a_{Crd})^{2.6} \times (a_{Spr})^{0.2}]/[(a_{Opx})^{3.3}]$.

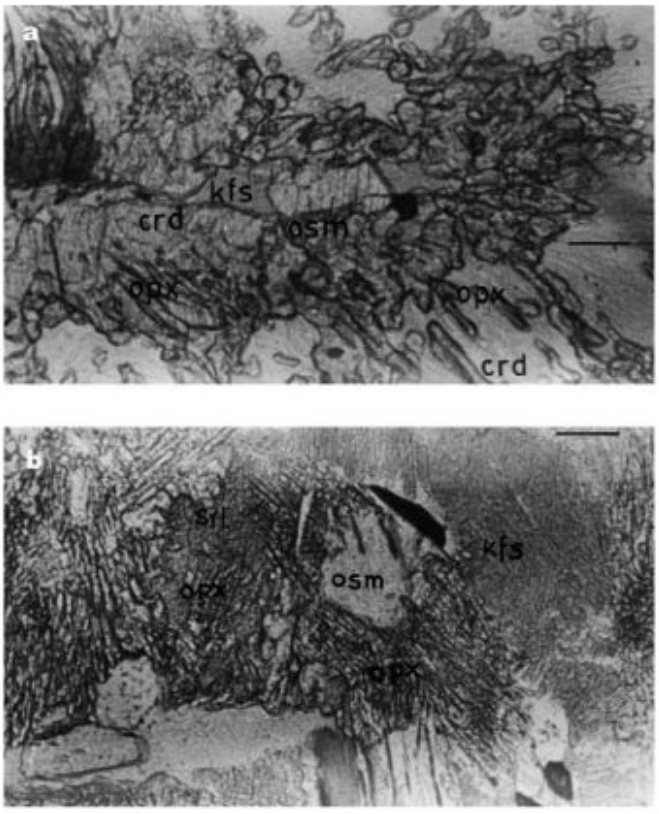

Fig. 5a, b. Photomicrographs (*scale bars* = 13 μ). **a** Symplectitic intergrowth of cordierite-orthopyroxene-K-feldspar enclosing relict osumilite. **b** Symplectitic intergrowth of orthopyroxene-sillimanite-K-feldspar enclosing relict osumilite

Reaction 3.

$$T\ (^{\circ}K) = [12.92 \times P + 6{,}240]/[114.98 + 8.313 \times \ln k],$$
where $k = [(a_{Opx})^2 \times (a_{Spr})^2]/(a_{Crd})^9$.

Reaction 4a.

$$T\ (^{\circ}K) = [29{,}760 + 5.59 \times P]/[98.1 - 8.313 \times \ln k],$$
where $k = (a_{Spr})/(a_{Spl})^7$.

Reaction 4b.

$$T\ (^{\circ}K) = [12.1 \times P - 11{,}760]/[106.54 - 8.313 \times \ln k],$$
where $k = (a_{Spr})/[(a_{Spl})^5 \times (a_{Opx})]$.

In Table 10 we give the balanced metamorphic reactions with relevant assemblages and phase compositions.

In Fig. 6 reactions 1 to 4a, b are positioned using the new calibrations presented in this study. For consistency, reactions 1, 2 and 3 in the assemblage P-II, reactions 4a and 4b in the assemblage P-IIIb, and reactions 5 and 6 from assemblages P-IIIc and P-IIIb respectively are only depicted here. Reaction 5 is said to be insensitive to pressure (Grew 1982). With the new experimental data of Holland et al. (1996), this reaction is found to have a steep positive slope of 86° in P–T space. Also, the (osm) invariant point in the KFMASH system (Carrington and Harley 1995b; Holland et al. 1996) is located at 900 °C, 8.7 kbar. Reaction 6 is said to have a steep positive slope in P–T space (Grew 1982) and, with experimental data of Holland et al. (1996), is found to have a slope of 76°.

Table 9. Thermodynamic parameters used for Mg end members

	$H_{(1,000\ ^{\circ}C,\ 1\ bar)}$ (kJ)	$S_{(1,000\ ^{\circ}C,\ 1\ bar)}$ (J)	$V_{(1,000\ ^{\circ}C,\ 6\ kb)}$ (J/bar)
Sapphirine 7:9:3	–21,153.68	2,683.94	51.64
Mg cordierite	–8,724.85	1,137.85	23.13
Enstatite	–2,934.04	392.82	6.26
Spinel	–2,189.29	268.85	4.01
Sillimanite	–2,465.81	295.20	5.01
Quartz	–867.27	113.49	2.27

Bulk-rock compositions

Major- and trace-element analyses by XRF spectrometry were carried out at the University Science Instrumentation Center, Gwahati University, India. At the Gwahati University, a Philips PW 1480 XRF spectrometer with a site window X-ray tube and software capable of calculating online matrixes and overlap interference was used. Average precision is always better than 1.5%. The overall accuracy (% RSD) for major and minor oxides is better than 5%, and for trace elements better than 12%. The analytical data for 14 metapelites and 16 granitoids are given in Tables 11 and 12.

In the molar [Al:(Na + K):(Fe + Mg)] plot the three metapelitic assemblages could be differentiated, indicating pelitic precursor of different bulk composition (Fig. 7). Also, the presence of greywacke-like precursors is indicated by some rocks with subequal Al:(Na + K) proportions.

In normative classification the granitoids of the study area are clearly of two types; most of them, garnet and spinel-bearing ones (G-I and G-II), are granites whereas some are of granodioritic composition (G-III) and can be described as quartz-monzonite in terms of their normative feldspar ratios (Fig. 8). However, both varieties are peraluminous with normative corundum (0.7 to 2.1%). Moreover, A/CNK values vary within a narrow range (0.86–1.11), indicating very little feldspar fractionation.

The petrogenesis of the peraluminous granitoids (G-I, G-II and G-III) which are produced by dehydration melting is best described in terms of the M–N–K pseudoternary phase diagram (after Patino Douce and Johnston 1991; Fig. 9). Here, many of the samples cluster around the invariant point I_2, whereas some are variably shifted towards M, presumably due to variable amounts of peritectic phases like garnet and spinel. Quartz monzonites (G-III) are plotted to the left of I_2 and, in line with the phase relations presented in Patino Douce and Johnston (1991), must have exhausted biotite before plagioclase – in other words, the protoliths of these granitoid rocks were plagioclase-rich. Here it is

Table 10. Balanced metamorphic reactions; phase compositions from Tables 1, 2, 3, 4, 5, 6, 7, and 8

Reaction no.	Balanced reaction	Assemblage	Sample no. (reference no.)
1	$Opx_{78} + 2\ Sil + Qtz = Crd_{92}$	P-II	97/31b (C1: opx, crd)
	$Opx_{81} + 2\ Sil + Qtz = Crd_{91}$	P-IIIa	97/46b (C2: opx, crd)
2	$3.3\ Opx_{78} + 7\ Sil = 2.6\ Crd_{83} + 0.2\ Spr_{83}$ (7:9:3)	P-II	95/10c (C5: opx, crd, spr)
	$3.3\ Opx_{84} + 7\ Sil = 2.6\ Crd_{93} + 0.2\ Spr_{86}$ (7:9:3)	P-IIIa	97/46b (C3: opx, crd, spr)
3	$9\ Crd_{90} = 2\ Opx_{81} + 2\ Spr_{82} + 35\ Qtz$	P-II	95/10c (C1: opx, crd, spr)
	$9\ Crd_{94} = 2\ Opx_{83} + 2\ Spr_{86} + 35\ Qtz$	P-IIIa	97/46b (C1: opx, crd, spr)
4A	$7\ Spl_{53} + 2\ Sil + Qtz = Spr_{80}$	P-IIIb	97/49 (C2: spl, spr)
	$7\ Spl_{53} + 2\ Sil + Qtz = Spr_{78}$	P-IIIc	95/15c (C1: spl, spr)
4B	$5\ Spl_{53} + Opx_{74} + 4\ Sil = Spr_{78} + 3\ Qtz$	P-IIIb	97/49 (C2: spl, spr, opx)
	$5\ Spl_{53} + Opx_{78} + 4\ Sil = Spr_{80} + 3\ Qtz$	P-IIIc	95/15c (C1: spl, spr, opx)
5	$3\ Osm_{81} = Opx_{74} + 2\ Crd_{89} + 3\ Kfs + 7\ Qtz$	P-IIIc	97/49 (C4: opx, kfs, crd, osu)
6	$Osm_{74} = Opx_{74} + 2\ Sil + Kfs + 3\ Qtz$	P-IIIb	95/15c (C1: opx, kfs, osu)

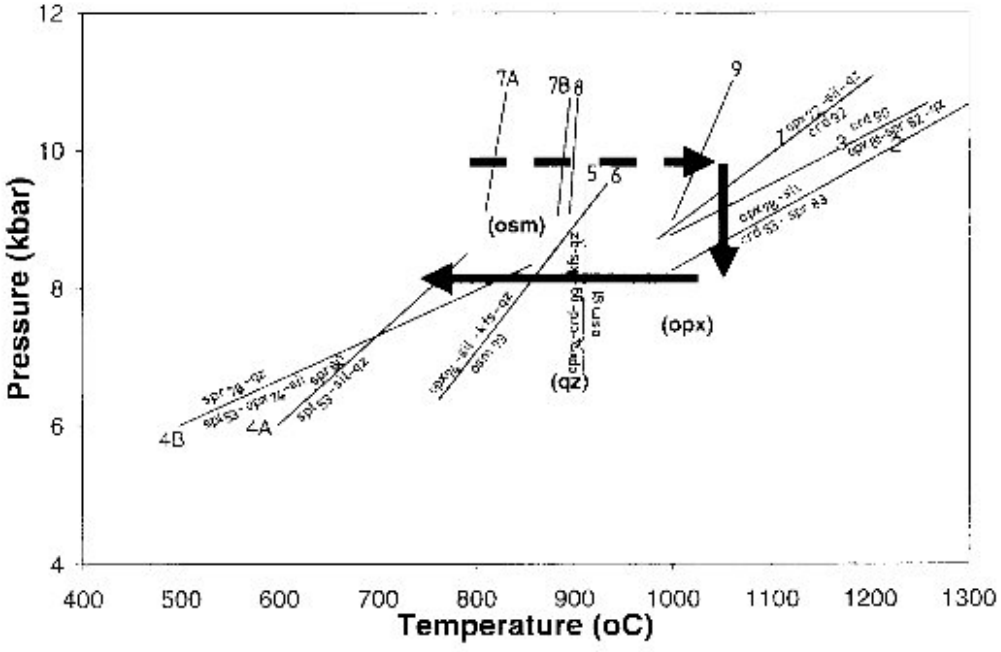

Fig. 6. Pressure-temperature path for the granulite complex of the present study area. Biotite melting solidus (*7A*) and biotite-out curve (*7B*) for pelite melting, and biotite-out curve (*8*) for greywacke melting are constrained from experimental data in Stevens et al. (1997). High-Mg pelite melting solidus (*9*) constrained from experimental data in Carrington and Harley (1995a). Invariant points (osm), (opx) and (qz) positioned from the experimental data in the KFMASH system provided by Carrington and Harley (1995b), and Holland et al. (1996)

important to recall that, although rare, khondalites in the area locally contain excess plagioclase, as in sample no. 97/88 whose trace-element signature is also distinctive and could imply the presence of greywacke-like precursor rocks.

The trace-element distribution between the garnet-rich and plagioclase-poor restites (P-I, except sample 97/88) and the peraluminous granitic melts (G-I and II) is depicted in the multi-element spider plot of Fig. 10. The granites are distinctly enriched in K and Rb, and depleted in Ti, Ni and Zn relative to the restites. However, Sr and Ba do not show significant enrichment in the granitic melts relative to the restites. The presence of significant K-feldspar (with high Ba and Sr K_D for mineral melt) in the restites (P-I), consistent with experimental observations (Stevens et al. 1997), could have caused the relative impoverishment of Sr and Ba in the melts.

The high-Mg (P-II) restites, on the other hand, are comparable with the quartzofeldspathic migmatitic layers (P-III), which could be interpreted as products of high-temperature melting in high-Mg pelitic precursors. The multi-element spider plot (Fig. 11) shows depletion of K and Rb in the migmatites relative to the restites (P-II), which incidentally contain significant amount of high-Mg restitic biotites. On the other hand, comparable Ba and variable Sr contents possibly reflect abundant peritectic K-feldspar in the migmatites and its paucity in the restites.

The variable Y and Zr contents in the granites, as compared with near-constant contents in the restites (Fig. 10), possibly reflect disequilibrium. Zr in the granitoids varies between 21 and 427 ppm. Zr values between 314 and 427 ppm (four samples) are close to Zr saturation in peraluminous granitic melts at temperatures ≥850 °C (Watson 1988). On the other hand, extremely low Zr (21, 38, 58, 70 ppm) would suggest rapid melt segregation, thereby causing lack of equilibration with restitic zircons, as suggested by Sawyer (1991).

Table 11. Bulk composition of metapelitic granulites

Rock type	P-I					P-II			P-III					
Sample no.	97/53	97/20a	97/88	95/18	97/60a	97/31a	97/31b	95/10c	95/15c	97/49	97/46a	97/46b	97/11	97/47
Ref. no.	P-1	P-2	P-3	P-4	P-5	P-6	P-7	P-8	P-9	P-10	P-11	P-12	P-13	P-14
SiO_2	74.96	65.2	70.59	63.15	66.59	44.05	45.6	43.58	61.52	74.69	74.26	71.2	69.7	72.2
Al_2O_3	12.84	18.16	14.55	18.45	18.36	21.2	21.31	22.63	17.56	14.76	13.27	14.61	14.51	14.15
Fe_2O_3	6.24	9.75	5.26	8.35	8.28	6.08	7.48	5.81	10.06	2.94	2.97	2.95	3.72	3.36
MnO	0.04	0.15	0.09	0.14	0.11	0.07	0.08	0.07	0.11	0.01	0.04	0.02	0.03	0.02
MgO	0.15	0.46	0.15	1.21	0.18	21.55	17.83	21.23	5.72	2.28	4.2	5.07	0.15	4.07
CaO	0.1	0.09	1.93	1	0.12	0.05	0.52	0.02	0.1	0	0.08	0.06	1.38	0.13
Na_2O	0.1	2.12	3.47	2.01	1.81	0.6	1.07	0.47	1.55	1.83	2.01	2.14	3.44	2.18
K_2O	2	1.7	3.36	3.35	2.85	4.75	4.09	4.84	1.91	2.12	1.85	2.26	6.19	2.6
TiO_2	1.29	1.42	0.48	1.05	1.04	1.5	1.59	1.54	0.99	0.24	0.65	0.71	0.57	0.68
P_2O_5	0	0.03	0.12	0.1	0.05	0.08	0.08	0.09	0.06	0.04	0.12	0.1	0.49	0.09
LOI	2.1	1.5	0.7	0.9	1.2	0.7	0.8	0.5	1.1	1.3	1.1	1.4	0.6	1.1
Total	99.67	100.58	100.7	99.71	100.59	100.63	100.45	100.78	100.68	100.21	100.55	100.52	100.78	100.58
Mg. no.	9	8	10	36	8	93	90	94	69	75	85	87	14	83
Trace element (ppm)														
Rb	33	37	97	81	74	216	228	198	124	54	89	97	314	102
Sr	62	51	143	99	45	5	50	5	7	5	5	17	71	24
Ba	672	502	762	1,135	624	359	338	321	246	471	597	471	480	379
Co	78	99	79	109	80	54	50	47	79	83	72	44	77	62
Ni	13	19	6	5	12	34	26	31	12	5	5	5	5	7
Zn	42	87	18	70	77	50	66	45	5	5	10	11	5	11
Y	29	64	131	56	48	47	39	33	109	48	89	89	141	97
Zr	616	367	185	274	268	405	416	392	175	124	336	393	379	394

Model melting reactions

The granitoid composition and mineralogy, the presence of high-Mg biotite in the high-Mg-Al sapphirine granulites as well as in the granitoids, and the presence of Opx–Crd–Osm assemblages in the leucocratic layers (P-III) are all suggestive of biotite dehydration melting in pelitic and greywacke-like precursors of magnesian bulk composition.

In their dehydration melting experiments, Stevens et al. (1997) used pelitic and greywacke starting materials both with highly magnesian biotite and, in view of the highly magnesian biotite in the present granitoids (X_{Mg} = 0.75–0.77 in G-I; 0.80–0.90 in G-II), this set of experiments is thought to be of special importance for the present granitoids.

From pelite melting experiment with a starting material $28Bio_{81} + 28Sil + 15Plg + 28Qtz$, Stevens et al. (1997) suggested a biotite melting reaction such as

$$Bio + Qtz + Plgl + Sil = Kfls \pm Grt \pm Crd + melt + Plg2 \quad (7)$$

and, from a greywacke melting experiment with a starting material $39Bio_{81} + 21Plg + 39Qtz$, these authors suggested a reaction such as

$$Bio + Qtz + Plgl = Kfls \pm Grt \pm Crd + Opx + melt + Plg2 \quad (8)$$

With the experimental P–T constraints, biotite melting solidus and biotite-out curves for pelite melting and biotite-out curves for greywacke melting are annotated 7a, 7b and 8 respectively in Fig. 6.

For the present granitoids these model melting reactions are thought to have special importance for the following reasons. First, the presence of highly magnesian biotite, although it could be restitic, in both the granite types (G-I and G-II) suggests a pressure-temperature domain which could be constrained by the biotite melting solidus (7a) and biotite-out curve (7b) of the pelite melting experiments. Second, granite with spinel (G-II), instead of garnet, is compatible with the high-temperature run products in the pelite melting experiments. In terms of the pseudoternary phase diagram of Patino Douce and Johnston (1991), the appearance of peritectic spinel in place of garnet also attests to melting temperatures above 850 °C. Incidentally, high-sanidine/anorthoclase feldspars are also observed in these granitoids and could reflect relatively higher temperature of melting or crystallization. Third, quartz-monzonite (G-III), thought to be the product of biotite melting in greywacke-like precursors, mostly lacks prograde biotite and hence could be constrained by the biotite-out curve (8) of the greywacke melting experiments.

In view of the presence of an Opx–Sil–Crd–Osm assemblage in some quartzofeldspathic layers, the melting experiments of Carrington and Harley (1995a) on high-Mg metapelites (with bulk X_{Mg} of starting materials = 0.60, 0.75, 0.90) are thought to have special bearing. Orthopyroxene, cordierite and osumilite phase compositions from the present study area, namely Opx_{75}, Crd_{89} and Osm_{81} (in P-III), are comparable to those produced in these experiments: Opx_{79}, Crd_{88} and Osm_{91}, at 1,000 °C and 9-kbar pressure in equilibrium

Table 12. Composition of granitoids of the Paderu, Andhra Pradesh

Rock type	G-I							G-II						G-III		
Sample no.	97/77	95/2	95/1a	95/3	97/86	97/40	97/110	97/17a	97/16a	95/35b	97/21	97/12b	97/67	97/22	97/8b	97/3
Ref. no.	G-1	G-2	G-3	G-4	G-5	G-6	G-7	G-9	G-10	G-11	G-12	G-13	G-8	G-14	G-15	G-16
SiO_2	74.05	73.14	70.05	71.84	70.6	69.49	71.35	77.62	72.63	76.59	74.45	66.14	75.38	64.54	69.36	71.84
Al_2O_3	12.55	13.41	14.96	13.48	14.38	15.17	12.14	10.68	14.17	12.16	14.21	12.93	13.12	16.9	13.32	13.45
Fe_2O_3	3.49	2.11	3.32	3.75	3.34	2.24	5.25	2.41	1.81	1.05	1.37	9.85	0.89	2.73	6.22	3.65
MnO	0.04	0.02	0.06	0.04	0.04	0.06	0.05	0.04	0.005	0.005	0.01	0.1	0.005	0.04	0.08	0.04
MgO	0.15	0.15	0.86	0.85	0.15	0.15	0.41	0.15	0.15	0.15	0.15	0.72	0.15	0.15	0.81	0.85
CaO	1.18	0.79	3.21	2.64	1.89	1.56	1.85	0.7	0.93	1.13	0.78	2.14	0.57	1.26	2.33	2.64
Na_2O	3.45	3.25	3.14	3.5	3.6	3.09	3.13	3.34	3.42	3.46	3.35	2.95	3.57	3.31	3.1	3.4
K_2O	5.03	6.8	3.57	1.83	4.91	7.37	4.22	5.11	6.29	5.26	5.45	3.09	6.03	9.46	2.89	1.83
TiO_2	0.32	0.16	0.3	0.61	0.58	0.09	1.05	0.23	0.19	0.15	0.09	1.18	0.17	0.37	0.64	0.61
P_2O_5	0.12	0.18	0.03	0.28	0.25	0.25	0.09	0.1	0.23	0.07	0.18	0.51	0.18	0.35	0.12	0.28
LOI	0.5	0.8	1.1	0.9	0.6	1.1	0.7	0.4	0.9	0.9	0.8	0.8	0.7	1.4	0.7	1.1
Total	100.88	97.56	100.6	99.72	100.34	100.57	100.24	100.78	100.73	100.93	100.84	100.41	100.77	100.51	99.57	99.69
Mg. no.	15	22	51	47	15	21	24	20	25	36	30	22	40	18	34	48
A/CNK	0.94	0.95	1.00	1.07	0.98	0.95	0.93	0.86	1.00	0.90	1.11	1.07	0.98	0.94	1.07	1.09
Trace elements (ppm)																
Rb	167	286	180	126	188	285	152	198	268	153	118	159	357	392	137	116
Sr	77	70	50	212	10	255	103	36	78	142	93	75	49	112	73	95
Ba	992	406	333	1,053	547	1,400	367	488	352	884	337	651	205	1,091	883	116
Co	63	110	95	110	88	80	68	75	66	80	111	86	90	73	102	51
Ni	8	5	5	8	5	5	16	5	5	6	0	5	5	5	13	7
Zn	18	7	11	17	13	9	91	16	5	20	5	5	5	12	38	5
Y	133	65	69	106	131	28	14	139	56	9	8	109	6	144	56	200
Zr	181	70	277	201	388	21	324	163	99	135	38	314	58	234	113	427

with granitic melts. Notably, the 9-kbar pressure is the lower limit of this melting reaction in these experiments. Accordingly, a model melting reaction, with phase compositions from this study, can be written as:

$$Bio_{86} + Sil + Qtz \pm Pl = Melt + Osm_{81} + Opx_{78-80} + Crd_{89} + Sil \quad (9)$$

In P–T space this reaction can be positioned from experiment nos. 47 and 65 of Carrington and Harley (1995a), and is depicted as reaction 9 in Fig. 6.

Pressure-temperature-time path

For reactions 1 to 3, the sense of reaction suggests decompression. Two other criteria for this decompressive P–T trajectory are the rimward decrease of Al_2O_3 in orthopyroxene, as shown by Montel and Vielzeuf (1997), and the fact that the early orthopyroxene (reactant phase in reaction 1) and those produced by cordierite breakdown (as in reaction 3) have the same X_{Mg} values, as expected on a decompressive P–T trajectory.

Sapphirine produced from spinel (as in reactions 4a and 4b) is much less magnesian than that produced from early orthopyroxene-cordierite association (as in reactions 2 and 3). Although a bulk compositional control is apparent, the migmatitic spinel-bearing assemblages (P-III) are thought to have been produced by high-temperature melting in high-Mg metapelites, as in the experiments of Carrington and Harley (1995a). This suggests that the late sapphirine-forming reactions were triggered by cooling. Although these reactions have gentle slopes in P–T space, with sapphirine on the higher pressure side, the alternative interpretation of a pressure rise seems unlikely because orthopyroxene in this assemblage (P-III), which is involved in the formation of late sapphirine (as in reaction 4b), is also less magnesian than those in the spinel-absent assemblage (P-II) and hence supports a cooling path (Fig. 6). Because of their near-vertical slopes, osumilite breakdown reactions are clearly indicative of cooling. Moreover, the relative dP/dT slopes of these reactions and change of osumilite composition between them indicate cooling at pressures below the intersection of reactions 5 and 6.

Thus, a post-peak path is interpreted to start with a decompression from ~10 to ~8 kbar at ~1,000 °C, and end in a prolonged cooling arm from above 900 to ~600 °C at ~8 kbar (Fig. 6). It is important to note that high-temperature decompression followed by cooling was described from two other areas in the Eastern Ghats granulite belt (Sen et al. 1995; Mohan et al. 1997).

The melting reactions 7, 8 and 9 in different pelitic and greywacke precursors, producing the granitoids and migmatitic magnesian pelitic gneisses, occurred at pressures above 9 kbar and at temperatures between 850 and 1,000 °C. As in the case of magnesian pelitic migmatites from Long Point, Raur group, Antarctica (Harley and Fitszimons 1991; Carrington and Harley 1995a), we interpret the migmatitic Opx–Crd–Sil–Osm ± Spl ± Spr-bearing quartzofeldspathic layers as products of high-temperature melting in magnesian pelitic rocks. Biotite, although possibly secondary or more likely of restitic origin, is highly magnesian (X_{Mg} = 0.86 to 0.90) and this additionally supports the contention that magnesian pelitic precursors were

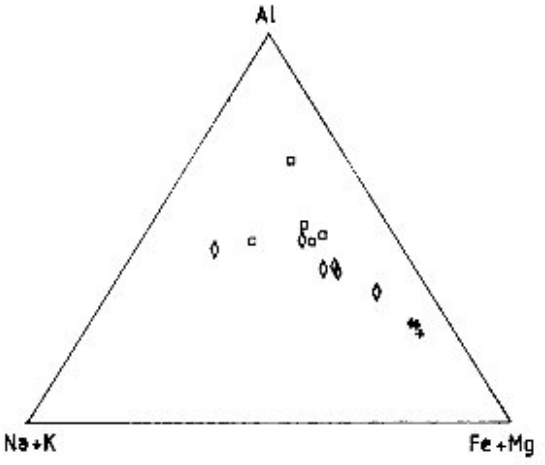

Fig. 7. Metapelites plotted on Al–(Na + K)–(Fe + Mg) diagram (molar). *Open square* Khondalites (P-I). + High-Mg metapelites (P-II). *Diamond* Intermediate-Mg metapelites (P-III)

present in the area, and are now represented by the restitic high-Mg pelitic assemblages Opx–Crd–Spr–Sil ± Qtz.

The high-temperature melting in high-Mg pelitic precursor above 9 kbar could represent the prograde arm and, together with the high-temperature decompression, describe a clockwise P–T-t path. It should be noted that the P–T vectors are all derived from high-Mg-Al restites and Osm–Crd–Opx restitic assemblage coexisting with granitic melt which are produced together during a high-temperature melting event.

Discussion

For the Eastern Ghats granulite terrain two types of P–T path have been reported, but their implications for the tectonic evolution of the terrain are not fully understood. Sengupta et al. (1990) related the counter-clockwise P–T path with "a compressive orogeny that was associated with high heat influx through mafic magmatism". According to these authors granulite metamorphism in the Eastern Ghats belt was caused by magmatic underplating, as in the model of Bohlen (1987). However, from thermal model constraints Mareschal (1994) indicated that "intrusion of significant magma into the lithosphere is unlikely in a compressional context". From detailed structural studies in several sectors of the Eastern Ghats belt, Bhattacharya (1997) argued that crustal thickening resulted from homogeneous shortening in a compressional setting, with no evidence of significant magmatic addition. Earlier, Mukherjee (1989) proposed that granulite metamorphism in the Chilka area was caused by anorthosite magmatism. Bhattacharya et al. (1994) argued on structural grounds that anorthosite magmatism was post-F_2 in the enclosing granulitic country rocks and hence could not be responsible for the granulite metamorphism in the area. Recently, Krause et al. (1998) argued, on the basis of

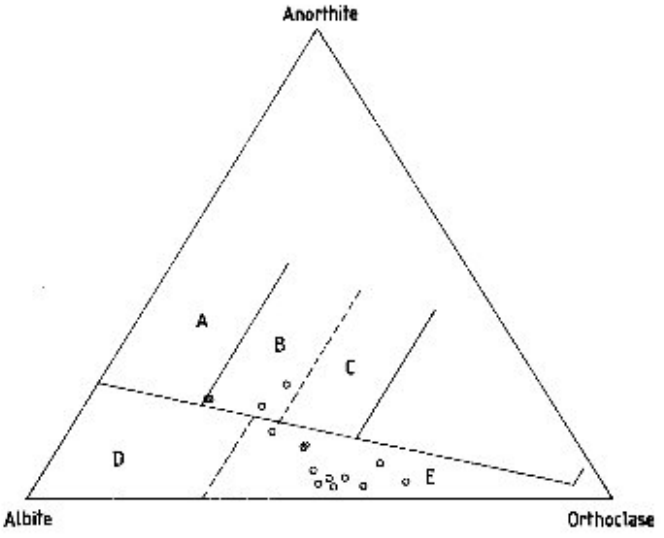

Fig. 8. Granitoids plotted on normative An–Ab–Or diagram. *E* Granite, *B+C* granodiorite, *A* tonalite, *D* trondhjemitic (after O'Connor 1965)

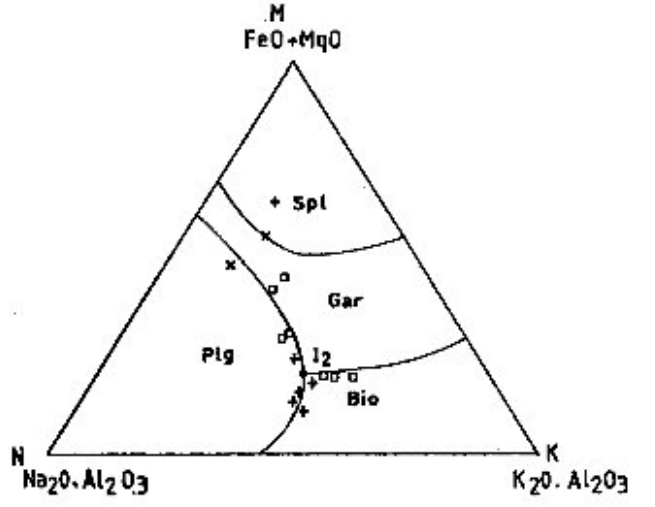

Fig. 9. Granitoids plotted on M–N–K pseudoternary diagram (after Patino Douce and Johnston 1991). *Open square* G-I, + G-II, *cross* G-III

isotopic evidence, that anorthosite "emplacement even postdates the last episode (Grenvillian) of granulite facies metamorphism in the Eastern Ghats belt ...".

On the other hand, a clockwise P–T path, as described here and in two other studies (Sen et al. 1995; Mohan et al. 1997), is compatible with the tectonic model proposed by Bhattacharya (1997), i.e. crustal thickening and granulite metamorphism in the Eastern Ghats belt resulted from homogeneous shortening in a compressional setting. In particular, the clockwise P–T-t path presented here implies crustal thickening-related heating as the cause of dehydration melting in high-Mg-Al pelitic rocks.

Now that both clockwise and counter-clockwise P–T paths are reported from different parts of the Eastern

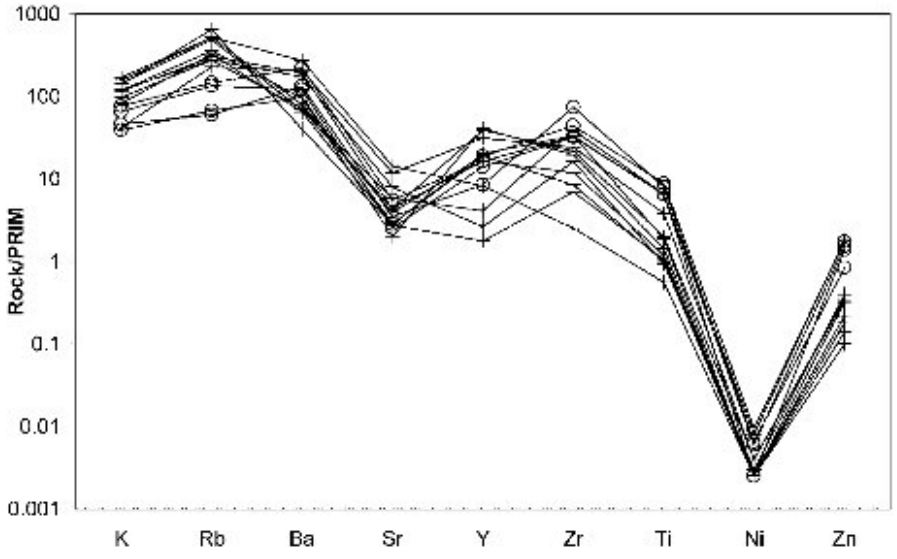

Fig. 10. Trace-element distribution between granitoids (G-I and II; +) and common khondalitic restites (P-I; *circles*) in a multi-element spider plot. Normalisation according to Taylor and McLennan (1985)

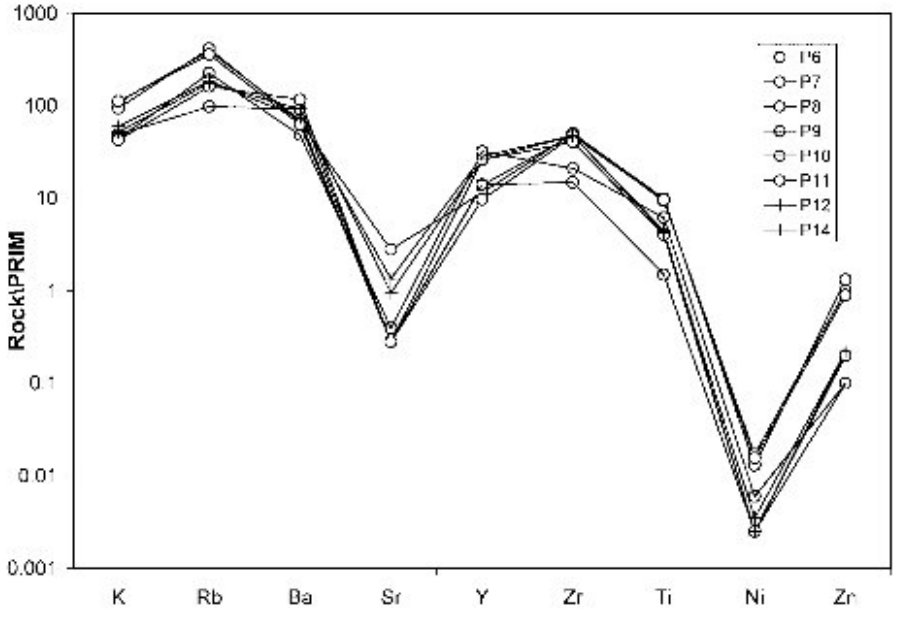

Fig. 11. Trace-element distribution between migmatites (P-III; +) and high-Mg restites (P-II; *circles*) in a multi-element spider plot. Normalisation according to Taylor and McLennan (1985)

Ghats granulite belt, one wonders how this can be incorporated in a single tectonic model for the entire Eastern Ghats belt.

Here, two important questions should be addressed. First, whether the reported contrasting P–T paths are only apparent P–T paths. It was already recognised that terrains with polyphase deformation and complex metamorphic record may sometimes display apparent P–T paths, which actually link P–T vectors from isotopically distinct metamorphic cycles (Barton et al. 1994). It is imperative, therefore, to consider only those P–T vectors recorded from petrologically related, if not isotopically dated, entities or assemblages. In other words, definite evidence should be provided to show that the assemblages evolved in a single metamorphic cycle. Unfortunately, however, Sengupta et al. (1990) could not provide definite evidence that "sapphirine granulite and the closely associated charnockite and mafic granulite" which were taken to "define an anticlockwise P–T trajectory" were in fact evolved together in a single metamorphic cycle. Here it is important to note that isotopic records in the Eastern Ghats belt point to several periods of granulite facies metamorphism (Shaw et al. 1997; Mezger and Cosca 1999; Bhattacharya et al. 2001).

Second, could the contrasting P–T paths reported from different sectors of the Eastern Ghats belt reflect the existence of different lithotectonic units? Some isotopic records from the Eastern Ghats granulite belt definitely indicate the presence of different crustal provinces or lithotectonic units (Bhattacharya et al. 2001). Hence, it is quite likely that contrasting P–T paths, if not apparent, may represent different lithotec-

tonic units or crustal provinces with unconnected pre-metamorphic history within the convergent orogen of the Eastern Ghats granulite belt.

Concluding remarks

The impress of early deformation structures in the high-Mg-Al sapphirine granulites here, together with the record of high-temperature decompression preceding isobaric cooling, is consistent with a clockwise P–T path. High-temperature melting producing the granitoids and migmatitic gneisses could represent the prograde arm of the clockwise P–T path. All the P–T records here are from high-Mg-Al restites and Osm–Crd–Opx restitic assemblage coexisting with granitic melt which are produced together during a high-temperature melting event. The clockwise P–T path is interpreted here as the result of crustal thickening-related heating and dehydration melting in the granulite complex of Paderu in the Eastern Ghats belt, India.

Acknowledgements This work was partially supported by the Council of Scientific and Industrial Research, New Delhi. The Indian Statistical Institute provided the infrastructural facilities. The analytical work reported here was carried out at the University Science Instrumentation Centres of Roorkee University and Gwahati University. Critical comments and suggestions of two anonymous reviewers on an earlier version are thankfully acknowledged.

References

Barton JM, Holzer L, Kamber B, Doig R, Kramers JD, Nyfeler D (1994) Discrete metamorphic events in the Limpopo belt, southern Africa : Implications for the application of P–T paths in complex metamorphic terrains. Geology 22:1035–1038

Berman RG (1988) Internally consistent thermodynamic data for minerals in the system Na_2O–K_2O–CaO–MgO–FeO–Fe_2O_3–Al_2O_3–SiO_2–TiO_2–H_2O–CO_2. J Petrol 29:445–522

Bhattacharya S (1996) Eastern Ghats granulite terrain of India: an overview. J Southeast Asian Earth Sci 14:165–174

Bhattacharya S (1997) Evolution of the Eastern Ghats granulite belt of India in a compressional tectonic regime and juxtaposition against Iron Ore Craton of Singhbhum by oblique collision-transpression. Proc Ind Acad Sci 106:65–75

Bhattacharya S, Sen SK, Acharyya A (1994) The structural setting of the Chilka Lake granulite-migmatite-anorthosite suite with emphasis on the time relation of charnockites. Precambrian Res 66:393–409

Bhattacharya S, Kar R, Misra S, Teixeira W (2001) Early Archaean continental crust in the Eastern Ghats granulite belt, India: Isotopic evidence from a charnockite suite. Geol Mag (in press)

Bohlen SR (1987) Pressure-temperature-time paths and tectonic model for the evolution of granulites. J Geol 95:617–632

Brown M (1994) The generation, segregation, ascent and emplacement of granite magma. Earth Sci Rev 36:83–130

Carrington DP, Harley SL (1995a) Partial melting and phase relations in high-grade metapelites: an experimental petrogenetic grid in the KFMASH system. Contrib Mineral Petrol 120:270–291

Carrington DP, Harley SL (1995b) The stability of osumilite in metapelitic granulites. J Metamorph Geol 13:613–625

Dasgupta S, Sengupta P, Fukuoka M, Chakraborti S (1992) Dehydration melting, fluid buffering and decompressional P-T path in a granulite complex from the Eastern Ghats, India. J Metamorph Geol 10:777–788

Dawson JB, Harley SL, Rudnick RI, Ireland TR (1997) Equilibration and reaction in Archaean quartz-sapphirine granulite xenoliths from the Lace kimberlite pipe, South Africa. J Metamorph Geol 15:253–266

Grew ES (1982) Osumilite in the sapphirine-quartz terrane of Enderby Land, East Antarctica: implications for osumilite petrogenesis in the granulite facies. Am Mineral 67:762–787

Harley SL (1984) The solubility of alumina in orthopyroxene coexisting with garnet in FeO-MgO–Al_2O_3–SiO_2 and CaO–FeO–MgO–Al_2O_3–SiO_2. J Petrol 25:665–696

Harley SL (1998) Ultrahigh temperature granulite metamorphism (1050 °C, 12 kbar) and decompression in garnet (Mg 70)-orthopyroxene-sillimanite gneisses from the Raur Group East Antarctica. J Metamorph Geol 16:541–562

Harley SL, Fitzsimons ICW (1991) Pressure-temperature evolution of metapelitic granulites in a polymetamorphic terrane: the Raur Group, East Antarctica. J Metamorph Geol 9:231–243

Harley SL, Hensen BJ, Sheraton JW (1990) Two stage decompression in orthopyroxene-sillimanite granulites from Forefinger Point, Enderby Land, Antarctica: implications for the evolution of the Archaean Napier Complex. J Metamorph Geol 8:591–613

Holland TJB, Powell R (1990) An enlarged and updated internally consistent thermodynamic dataset with uncertainties and correlations: the system K_2O–Na_2O–CaO–MgO–MnO–FeO–Fe_2O_3–Al_2O_3–TiO_2–SiO_2–C-H_2–O_2. J Metamorph Geol 8:89–124

Holland TJB, Babu EVSSK, Waters DJ (1996) Phase relations of osumilite and dehydration melting in pelitic rocks: a simple thermodynamic model for the KFMASH system. Contrib Mineral Petrol 124:383–394

Krause O, Mezger K, Raith M (1998) Age constraints on the emplacement of massif-type anorthosites in the Eastern Ghats belt, India. In: Int Sem Precambrian Crust in Eastern and Central India, IGCP (Bhubaneswar) 368:121–123

Kretz R (1983) Symbols for rock forming minerals. Am Mineral 68:277–279

Lal RK (1997) Internally consistent calibrations for geothermobarometry of high-grade Mg-Al rich rocks in the system MgO-Al2O3-SiO2 and their application to sapphirine-spinel granulites of Eastern Ghats, India and Enderby Land, Antarctica. Proc Ind Acad Sci 106:91–114

Lal RK, Ackermand D, Upadhyay H (1987) P-T-X relationships deduced from corona textures in sapphirine-spinel-quartz assemblages from Paderu, southern India. J Petrol 28:1139–1168

Mareschal J (1994) Thermal regime and post-orogenic extension in collision belts. Tectonophysics 238:471–484

Mezger K, Cosca MA (1999) The thermal history of the Eastern Ghats Belt (India) as revealed by U–Pb and $^{40}Ar/^{39}Ar$ dating of metamorphic and magmatic minerals: implications for the SWEAT correlation. Precambrian Res 94:251–271

Mohan A, Windley BF (1993) Crustal trajectory of sapphirine-bearing granulites from Ganguvarpatti, South India: evidence for an isothermal decompression path. J Metamorph Geol 11:867–878

Mohan A, Tripathi P, Motoyoshi M (1997) Reaction history of sapphirine granulites and a decompressional P-T path in a granulite complex from the Eastern Ghats. Proc Ind Acad Sci 106:115–130

Montel JM, Vielzeuf D (1997) Partial melting of metagreywackes, part II. Compositions of minerals and melts. Contrib Mineral Petrol 128:176–196

Mukherjee A (1989) P-T-time history and thermal modelling of an anorthosite-granulite interface, Eastern Ghats metamorphic belt, India. In: Daly JS, Cliff RA, Yardley BWD (eds) Evolution of metamorphic belts. Geol Soc Spec Publ 43:265–274

Mukhopadhyay AK, Bhattacharya A (1997) Tectonothermal evolution of the gneiss complex at Salur in the Eastern Ghats granulite belt of India. J Metamorph Geol 15:719–734

Nichols GT, Berry RF (1991) A decompressional P-T path, Reinbolt Hills, East Antarctica. J Metamorph Geol 9:257–266

Nichols GT, Berry RF, Green DH (1992) Internally consistent gahnitic spinel-cordierite-garnet equilibria in the FMASHZn system: geothermobarometry and applications. Contrib Mineral Petrol 111:362–377

O'Connor JT (1965) A classification for quartz-rich igneous rocks based on feldspar ratios. US Geol Surv Prof Pap 525B:79–84

Patino Douce AE, Johnston AD (1991) Phase equilibrium and melt productivity in the pelitic system: implications for the origin of peraluminous granitoids and aluminous granulites. Contrib Mineral Petrol 107:2202–2218

Patino Douce AE, Johnston AD, Rice JM (1993) Octahedral excess mixing properties in biotite: a working model with application to geobarometry and geothermometry. Am Mineral 78:113–131

Raith M, Karmakar S, Brown M (1997) Ultra-high-temperature metamorphism and multistage decompressional evolution of sapphirine granulites from the Palni Hill Ranges, south India. J Metamorph Geol 15:379–399

Sawyer EW (1991) Disequilibrium melting and the rate of melt-residuum separation during migmatization of mafic rocks from the Grenville Front, Quebec. J Petrol 32:701–738

Schreyer W, Maresch WV, Daniels P, Wolfsdroff P (1990) Potassic cordierite: characteristic mineral for high-temperature, very low pressure environment. Contrib Mineral Petrol 105:162–172

Sen SK, Bhattacharya S (1997) Dehydration melting of micas in the Chilka Lake khondalites: The link between the metapelites and granitoids. Proc Ind Acad Sci 106:277–297

Sen SK, Bhattacharya S (2000) Diverse signatures of deformation, pressure-temperature and anatexis in the Rayagada sector of the Eastern Ghats granulite terrane. Proc Ind Acad Sci 109:347–369

Sen SK, Bhattacharya S, Acharyya A (1995) A multi-stage pressure-temperature record in the Chilka Lake granulites: the epitome of the metamorphic evolution of Eastern Ghats, India? J Metamorph Geol 13:287–298

Sengupta P, Dasgupta S, Bhattacharya PK, Fukuoka M, Chakraborti S, Bhowmik S (1990) Petro-tectonic imprints in the sapphirine granulites from Anantagiri, Eastern Ghats mobile belt, India. J Petrol 31:971–996

Shaw RK, Arima M, Kagami H, Fanning CM, Shiraishi K, Motoyoshi Y (1997) Proterozoic events in the Eastern Ghats belt, India: evidence from Rb–Sr, Sm–Nd systematics and SHRIMP dating. J Geol 105:645–656

Stevens G, Clemens JD (1993) Fluid-absent melting and the role of fluids in the lithosphere: a slanted summary? Chem Geol 108:1–17

Stevens G, Clemens JD, Droop GTR (1997) Melt production during granulite facies anatexis: experimental data from "primitive" metasedimentary protoliths. Contrib Mineral Petrol 128:352–370

Taylor SR, McLennan SM (1985) The continental crust: its composition and evolution. Blackwell, Oxford

Vielzeuf D, Montel JM (1994) Partial melting of metagreywackes. Part I. Fluid-absent experiments and phase relationships. Contrib Mineral Petrol 117:375–393

Vry JK, Brown PE, Valley JW (1990) Cordierite volatile content and the role of CO_2 in high-grade metamorphics. Am Mineral 75:71–88

Watson EB (1988) The role of accessory minerals in granitoid chemistry. In: Ist Hutton Meet The Origin of Granites and Related Rocks. Edinburgh, R Soc Edinburgh, Abstr Vol 1, pp 19–20